PCCP

Accepted Manuscript

ROYAL SOCIETY OF CHEMISTRY

www.rsc.org/pccp

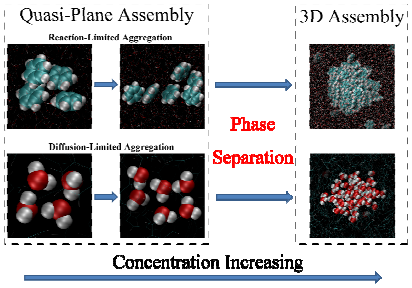

Difference of the molecular aggregations in benzene-water mixtures is identified by all-atom molecular dynamics simulations.

Different Aggregation Dynamics of the Benzene-Water Mixtures

Cen-Feng Fu and Shan Xi Tian*

Hefei National Laboratory for Physical Sciences at the Microscale and Department of Chemical Physics, University of Science and Technology of China, Hefei, Anhui 230026, China

* Corresponding author. E-mail: sxtian@ustc.edu.cn

Abstract

All-atom molecular dynamics simulations for the benzene-water mixtures are performed, aiming to explore the relationship between the microscopic structures and the thermodynamic properties, in particular, the transformation dynamics from the mutually soluble state to the phase-separated state. We find that the molecular aggregation of benzene in the water-rich mixture is distinctly different from that of water in the benzene-rich mixture. This aggregation difference is attributed to the different intermolecular interactions: the clustering of benzenes in the water-rich mixture is primarily driven by the weak short-distanced π-π interactions; while the formation of water cluster in the benzene-rich solution is triggered by the long-range dipole-dipole electrostatic interaction. Moreover, the molecular aggregations show the double-scaled features: firstly assembling in a quasi-plane at the low concentration, then bulking in three dimensions with the concentration increase.

1. Introduction

Hydrophobicity as a fundamental phenomenon plays an essential role in chemical and biological processes.[1-11] A lot of efforts have been devoted to understanding the nature of hydrophobic interactions.[12-16] Weak solubility of nonpolar solute in liquid water declines as temperature increases, indicating that the driving force of hydrophobicity is dominated by the adverse entropic contribution.[2, 4, 17, 18] The assembly or aggregation of hydrophobic units may be driven entropically for small molecules, but enthalpically for large clusters.[19-22] Benzene-water mixture is a particular interesting system, in which benzene molecule exhibits not only hydrophobicity but also weak hydrophilicity. Due to the spatial shape of molecular π-electron distribution, the weak hydrophilicity of benzene is attributed to an attractive interaction via hydrogen bond with water (O-H···π) in a region perpendicular to the benzene plane; while in the equatorial region, benzene acts as an ordinary hydrophobic solute in liquid water.[23-37] Moreover, this attractive O-H···π interaction energy (enthalpy) is responsible for the hydration free energy of benzene. In contrast, the typical hydrophobic effect of the aliphatic hydrocarbon-water system is induced by the adverse entropic contribution.[38] In the solvation of a benzene molecule into liquid water, the hydrogen bond net of waters is partly broken while the water-benzene O-H···π hydrogen bond is formed. It was found that the conversion of a water-water O-H···O hydrogen bond to a water-benzene O-H···π hydrogen bond was entropically favored but enthalpically disfavored.[39]

Thermodynamic and structural properties of one or several benzene molecules embedded in liquid water have been extensively investigated,[26-39] but very few studies are reported on

the mixtures where water molecules are immersed in liquid benzene.[40-43] According to our conventional wisdom, enough benzene molecules should aggregate in water; vice versa, a quantity of water molecules tend to accumulate in liquid benzene. However, the dynamic mechanisms of these two-directional aggregations are still not explicit,[44] in particular, the thermodynamic transformation from the mutually soluble state to the phase-separated state deserves systematic investigations. This should also be of great significance toward understanding of the nature of hydrophobicity.

In this work, using all-atom molecular dynamics (MD) simulation, we investigate the benzene-water liquid mixtures at different mole fractions (x_W and x_B), aiming to reveal the driving force of the benzene-water phase separation and to establish the relationship between the microscopic structures and the thermodynamic properties of the molecular aggregations.

2. Models and Methods

2.1 Molecular Dynamics Simulations.

The TIP4P model[45] and the OPLS-AA force field[46] were chosen for water and benzene, respectively. Their force filed parameters are given in Table 1. The reliability of the chosen force fields in describing the intermolecular interactions between two benzenes (parallel sandwich, perpendicular T- and Y-shaped) and between water and benzene (via O-H···π hydrogen bond) was examined. As shown in Figure 1, the positions and depths of the local minima in the potential energy profiles predicted with the force field parameters were quite

similar to those obtained with the high-level quantum chemistry calculations.[47, 48] Moreover, the OPLS-AA proved to be successful in the reproductions of both molecular structures and thermodynamic properties of liquid benzene.[49]

A series of the liquid mixtures at 21 different mole fractions were simulated. A summary about the different systems was given in Table 2. Firstly, the molecules were scattered randomly in the box; then the system was mixed well via annealing protocol and by an energy-minimized procedure. Subsequently, a 40.0 ns simulation was performed to equalize the system, followed by an additional 20.0 ns simulation for the product collection. The side length of box for the equilibrated systems was c.a. 8.54 ~ 9.97 nm. MD simulations were carried out using a time step of 1.0 fs in the *NPT* ensemble at P = 1 atm and T = 300 K. The Nosé-Hoover thermostat[50, 51] and Parrinello-Rahman isotropic barostat[52, 53] were employed to impose constant temperature and pressure, respectively. The periodic boundary conditions were applied in all three directions. The electrostatic interactions were treated by using the particle-mesh Ewald method[54] with a real space cutoff of 1.3 nm and the cutoff distance1.5 nm for the van der Waals interactions. All bonds were constrained using the P-LINCS algorithm.[55, 56] All simulations were performed with the GROMACS 4.5.5 package.[57]

2.2 The Kirkwood-Buff Analysis.

The relation between the microscopic structure and thermodynamic property of binary liquid can be derived on the basis of the Kirkwood-Buff (KB) theory.[58] The most fundamental

quantity is the KB integral (KBI),

$$G_{ij} = \int_0^\infty \left[g_{ij}(r) - 1 \right] 4\pi r^2 dr ,$$

where $g_{ij}(r)$ is the radial distribution function (RDF) between components i and j. This integral should be obtained for an open system, but in practice the KBI from a closed-boundary NPT or NVT simulation may suffer the convergence.[59, 60] This problem could be overcome with the benefits of recent works.[59, 60] Firstly, the RDF is corrected as[60]

$$g_{ij}^{correct}(r) = g_{ij}(r) \cdot \frac{N_j \left(1 - \frac{(4/3)\pi r^3}{V} \right)}{N_j \left(1 - \frac{(4/3)\pi r^3}{V} \right) - \Delta N_{ij}(r) - \delta_{ij}} ,$$

where N_j is the number of particle j in the system, V is the volume of the system, and $\Delta N_{ij}(r)$ is the excess number of particle j within a sphere of radius r around particle i; then, the KBI can be calculated by[59]

$$G_{ij}(R) = \int_0^{2R} \left[g_{ij}^{correct}(r) - 1 \right] \cdot \left(1 - \frac{3x}{2} + \frac{x^3}{2} \right) 4\pi r^2 dr$$

where $x = r / (2R)$. Physically, the KBI represents the volume difference for particle j in a sphere with a radius of R where the particle center changes from being chosen at a random point to being coincident with the center of particle i.

Using the KBI values, preferential solvation (PS) can be further estimated to characterize the structure of the mixture. In the binary system, the PS of a specific molecule i with respect to itself is calculated by[58]

$$PS(i \mid i) = \frac{x_i x_j \left(G_{ii} - G_{ij}\right)}{x_i G_{ii} + x_j G_{ij} + V_a},$$

where V_a is the volume of a sphere with a radius of a few molecular diameters; and the PS follows $PS(i|i) = -PS(j|i)$. The derivatives of the chemical potential (μ) at the constant temperature and pressure can be determined with the KBI values:

$$\left(\frac{\partial \mu_i}{\partial x_i}\right)_{T,P} = k_B T\left(\frac{1}{x_i} - \frac{\rho_j \Delta_{ij}}{1 + \rho_j x_i \Delta_{ij}}\right),$$

where k_B is the Boltzmann constant, and $\Delta_{ij} = G_{ii} + G_{jj} - 2G_{ij}$.[58]

2.3 Excess Enthalpy and Excess Entropy

The excess enthalpy (ΔH^{EX}) can be determined with the potential energy U,[61]

$$\Delta H^{EX} = U_{mix} - x_B U_B - x_W U_W,$$

where U_B and U_W are the potential energy of the pure benzene and water liquid, respectively. For the liquid, ΔH^{EX} is approximated to be the energetic difference (ΔU_{total}) between the mixture and the pure liquid(s) and decomposed as,

$$\begin{aligned} \Delta U_{total} &= x_B (U_{BB} - U_B) + x_W (U_{WW} - U_W) + U_{BW} \\ &= \Delta U_{BB} + \Delta U_{WW} + \Delta U_{BW} \end{aligned},$$

where U_{BW}, U_{BB}, and U_{WW} are the total benzene-water, benzene-benzene, and water-water interaction energies in the mixture, respectively. The excess entropy (ΔS^{EX}) is predicted within the two-particle approximation,[62]

$$\Delta S^{EX} = S_2^{EX} = -2\pi k_B \rho \sum_{i,i} x_i x_j \int \left[g_{ij}(r) \ln g_{ij}(r) - g_{ij}(r) + 1\right] r^2 dr.$$

3. Results and Discussion

3.1 Radial distribution functions

To evaluate the overall features about the structures of benzene-water mixtures with different mole fractions, we firstly calculated the RDF [$g(r)$] as function of the molecular center-of-mass. As illustrated in Figure 2, at the low concentrations of benzene (x_B = 0.0024, 0.0036, and 0.0049, see Figure 2a) and water (x_W = 0.0030 and 0.0050, see Figure 2f), the values of $g_{BB}(r)$ and $g_{WW}(r)$ are around 1.0 for r > 1.0 nm, exhibiting the appealing mutual solubility between two species. When x_B > 0.0049 or x_W > 0.0050, the $g(r)$ values are enhanced significantly in the region of r < 2.0 nm, implying the existence of molecular clusters. As shown in Figures 2c and 2d, the profile peaks of $g(r)$ are weakened gradually with the increase of x_B or x_W, signifying that the number of the water (benzene) molecules surrounding a benzene (water) molecule decreases, namely, the phase separation occurs. Moreover, one can find the monotone decrease of $g(r)$ for benzene-rich mixture (Figure 2d) is relatively slowly, while $g(r)$ for the water-rich mixture (Figure 2c) shows a sudden decrease around $x_B \sim 0.0050$. This prefigures that the aggregation dynamics of water molecules in benzene-rich mixture should be distinctly different from that of benzene molecules in water-rich mixture. On the other hand, as shown in Figures 2b and 2e, the aggregation hardly influences the profiles of $g_{BB}(r)$ and $g_{WW}(r)$, because the number of water or benzene molecules involved in this process is quite small.

3.2 KB Analysis

In Figure 3a, the G_{BB} (in the left) achieves the sharp growths when $x_B > 0.0049$, which is in line with the previous study.[44] The G_{WW} (in the right) also achieves the sharp growth when $x_W > 0.0050$ in the benzene-rich mixture. These variances of G_{BB} and G_{WW} mean that at the high x_B or x_W a further introduction of a benzene or water molecule at the center of a sphere will greatly raise the number of benzene or water molecules in this sphere. This is closely related to the molecular assembly in the mixture. In addition, all G_{BW} values are negative, and they decay with the increase of x_B (in the left) or x_W (in the right), implying that the interaction between benzene and water is generally repulsive although there is a hydrogen bond O-H$\cdots\pi$ in the specific spatial arrangement.

Defined as the difference between the local and global compositions around a molecule, the *PS* value further quantifies a detailed landscape of the local solvation around. As depicted in Figure 3b, the near-zero values of *PS*(B|B) in the water-rich mixture ($x_B < 0.0049$) indicate that benzene molecule does not prefer aggregation and thus the dilute aqueous solution of benzene is stabilized. However, when $x_B > 0.0049$, there is a sharp enhancement of *PS*(B|B), demonstrating a quick aggregation of benzene molecules. Meanwhile, the *PS*(W|W) value raises slightly with the x_B increase in the water-rich mixture. On the other hand, in the benzene-rich mixture, the *PS*(W|W) and *PS*(B|B) profiles show the reversed tendencies. With respect to the *PS*(B|B) in the water-rich mixture, the increase of *PS*(W|W) in the x_W range of 0.0050 - 0.0070 is relatively tardy. The microstructures at four representative mole fractions are shown in Figure 3c, vividly exhibiting the discrete state of the benzene in the dilute

aqueous solution (i), the sudden aggregation of benzene molecules (ii), and the development of water clusters (iii, iv).

The structural properties of the benzene-water mixtures have been revealed, on the basis of the results of RDF, KBI, and *PS*. With the increase of concentration, the aggregation of benzene in the water-rich mixture occurs more suddenly than that of water in the benzene-rich mixture. The thermodynamic properties of the mixture are further investigated in the following parts. In the KB theory, the derivatives of the chemical potential reflect the direction for the fluctuation of the local composition. $\partial\mu_i/\partial x_i > 0$ indicates that local composition has reached equilibrium, namely, μ_i increases with the increase of local x_i, meaning that molecule *i* should flow out of this local region and the equilibrium composition in this region is restored. In Figure 4a, in the water-rich mixture, the high positive values of $\partial\mu_B/\partial x_B$ for the much lower x_B (≤ 0.0049) show that the benzene distribution in its dilute solution is relatively stable in thermodynamics; $\partial\mu_W/\partial x_W$ shows a trend similar to that of $\partial\mu_B/\partial x_B$. In the benzene-rich mixture, the variances of $\partial\mu_W/\partial x_W$ and $\partial\mu_B/\partial x_B$ are in the similar scenarios, but the values of $\partial\mu_W/\partial x_W$ are much larger than $\partial\mu_B/\partial x_B$. In the water-rich mixture, the rapid decrease of $\partial\mu_W/\partial x_W$ or $\partial\mu_B/\partial x_B$ occurs around $x_B = 0.0050$, which is qualitatively in agreement with the previous study;[44] while the decrease of $\partial\mu_W/\partial x_W$ or $\partial\mu_B/\partial x_B$ for the benzene-rich mixture is relatively moderate. The reductions of these chemical potential derivatives imply that the solution equilibrium is being broken, in accord with the benzene-water phase separation illustrated in Figures 2 and 3.

3.3 Excess Enthalpy and Excess Entropy

Since there are arguments about the roles of enthalpy and entropy in the hydrophobicity,[2, 4, 17-22, 38, 39] here we calculate the ΔH^{EX} and ΔS^{EX} values to reveal the predominated incentive in the phase separation of the benzene-water mixtures. In Figure 4b, the ΔH^{EX} values are positive, while the ΔS^{EX} values are negative. The variance of ΔH^{EX} or ΔS^{EX} at the neighbourhood of x_B or x_W, i.e., $\Delta\Delta H^{EX}(x_1 \rightarrow x_2) = \Delta H^{EX}(x_2) - \Delta H^{EX}(x_1)$ or $\Delta\Delta S^{EX}(x_1 \rightarrow x_2) = \Delta S^{EX}(x_2) - \Delta S^{EX}(x_1)$, can directly characterize the driving force of the phase separation at the certain concentration. In the water-rich mixture, when $x_B < 0.0049$, $\Delta\Delta S^{EX} \approx 0$ and $\Delta\Delta H^{EX} > 0$, indicating that in the completely soluble system the entropy is almost unvaried while the enthalpy is still increasing. With the x_B increase, there is a small but quick jumpdown of ΔH^{EX} (i.e., $\Delta\Delta H^{EX} < 0$, see the inserted panel) from $x_B = 0.0049$ to 0.0050, then the ΔH^{EX} increases again; at the same time, the absolute value of ΔS^{EX} begins to continuously increase. Around $x_B = 0.0050$, the aggregation of benzene molecules occurs, thus this phase separation is somewhat reflected as the enthalpy change. The present finding is consistent with the previous conclusion.[20] In the benzene-rich mixture, the similar trends of the variations of ΔS^{EX} and ΔH^{EX} are observed. $\Delta\Delta S^{EX} \approx 0$ and $\Delta\Delta H^{EX} > 0$ at low x_W, while the remarkable variance of ΔH^{EX} is found for the water clustering. This implies that the aggregation of hydrophilic units in the hydrophobic liquid is also shown as the significant enthalpy change. However, the decreasing magnitude and range of ΔH^{EX} for the benzene clustering are much weaker and narrower than those for the water aggregation. Evidently, this distinct difference is attributed to their different aggregation dynamics.

Since above different aggregation dynamics is basically indicated as the enthalpy change, ΔH^{EX}, approximately equal to ΔU_{total} for liquids, deserves further investigation. The ΔU_{total} value and its three components (ΔU_{BB}, ΔU_{WW}, and ΔU_{BW}) consist of two physical contributions, i.e., Lennard-Jones (square label) and coulombic (circle label) interactions, as plotted in Figure 4c. These two contributions of ΔU_{BW} are the negative values, indicating that the attractive interaction between benzene and water (basically due to the O-H …π hydrogen bonding) is apt to stabilize the mixture. This attraction is largely weakened around x_B = 0.0050, which is witnessed as the sudden drops of the two contributions of ΔU_{BW} and corresponds to the aggregation of benzene in the water-rich mixture. Such phase separation is also found as the sharp changes of the Lennard-Jones interaction value of ΔU_{BB} and the coulombic interaction value of ΔU_{WW}. During the aggregation of benzene, the π-π interaction among the approaching benzenes[49] becomes much stronger than those among the dispersive benzenes; meanwhile, the aggregation of benzene results in the reconstruction of the hydrogen bond net of water, leading to the drastic change of the coulombic contribution ΔU_{WW}. On the contrary, in the benzene-rich mixture, the significant variances are only observed for the coulombic contributions of ΔU_{WW} (green circle / broken-line) and ΔU_{total} (black circle / solid-line), which is mainly attributed to the formation of water cluster around x_W = 0.005~0.010.

3.4 Aggregation Dynamics

To further investigate the molecular assembly dynamics in the aggregation processes, the size of clusters (M, number of molecules contained in a cluster) as functions of the radius of

gyration R_g is plotted in Figure 5. Assuming $M \propto R_g^{d_f}$ where d_f is the fractal dimension,[63] the two cluster-size dependent regions are clearly observed. These data are produced by using the microstructures of the equilibrium mixtures at different mole fractions. For the small water clusters (R_g < c.a. 0.3 nm), d_f = 1.78; and d_f = 2.33 for the small benzene clusters (R_g < c.a. 0.9 nm). As shown in the schematic diagrams of Figure 5, water molecules can be assembled by the hydrogen bonds in a nearly planar network, in which each water acts both the acceptor and donor of the hydrogen bonds. According to the previous findings, two benzene molecules can be stabilized as the nearly perpendicular configuration,[49] leading to a quasi-planar (layer-like) microstructure of the small benzene clusters. On the other hand, two scaling concepts, diffusion-limited aggregation (DLA) and reaction-limited aggregation (RLA),[64] are applicable to illustrate the aggregation processes of water and benzene, respectively. As discussed above, the molecular aggregations of benzene and water are commonly driven by the favorable enthalpy variance, but the dominated contributions to the enthalpy are the Lennard-Jones and coulombic interactions, respectively. Therefore, in the DLA model with the typical value of $d_f \approx 1.8$,[64] water molecules can gather more easily due to their long-range dipole-dipole attraction; while in the RLA model with the typical value of $d_f \approx 2.1$,[64] the aggregation of benzene molecules happens until overcoming the steric repulsion in their approaching. With the molecular number increase, the aggregation tends to develop in three dimensions, i.e., d_f = 3.19 for the larger benzene clusters and d_f = 3.08 for the larger water clusters, which is propitious to reduce the ratio of volume to surface area of the hydrophobic cluster.[20]

4. Conclusion

In summary, the structural and thermodynamic properties of benzene-water mixture have been investigated with the comprehensive MD simulations. The aggregation of benzene or water is primarily driven by the enthalpy variance. We further conclude that the aggregation dynamics of hydrophilic units in hydrophobic solvent is similar to that of hydrophobic units in hydrophilic solvent. Double-scaled dynamic features of the molecular aggregations are revealed here: firstly assembling molecules nearly in a quasi-plane at the low concentrations, and bulking in three dimensions with the concentration increase. Another significant finding is that the former process is further classified into: a RLA model for the clustering of benzene in the water-rich mixture, due to the short-distanced $\pi\cdots\pi$ intermolecular interactions of benzenes; while a DLA model for the formation of water cluster in the benzene-rich mixture, triggered by the long-range dipole-dipole interactions of water molecules.

Acknowledgments

This work is supported by CAS (Grant No. KJCX2-EW-W09) and FRFCU (Grant No. WK2340000012). The numerical calculations have been done on the supercomputing system in the Supercomputing Center of University of Science and Technology of China.

References

1. D. M. Huang and D. Chandler, *Proc. Natl. Acad. Sci. U. S. A.*, 2000, **97**, 8324-8327.

2. N. T. Southall, K. A. Dill and A. D. J. Haymet, *J. Phys. Chem. B*, 2002, **106**, 521-533.
3. R. L. Baldwin, *Science*, 2002, **295**, 1657-1658.
4. L. R. Pratt, *Annu. Rev. Phys. Chem.*, 2002, **53**, 409-436.
5. L. R. Pratt and A. Pohorille, *Chem. Rev. (Washington, DC, U. S.)*, 2002, **102**, 2671-2692.
6. E. Rabani, D. R. Reichman, P. L. Geissler and L. E. Brus, *Nature*, 2003, **426**, 271-274.
7. G. A. Papoian, J. Ulander, M. P. Eastwood, Z. Luthey-Schulten and P. G. Wolynes, *Proc. Natl. Acad. Sci. U. S. A.*, 2004, **101**, 3352-3357.
8. H. S. Ashbaugh and L. R. Pratt, *Rev. Mod. Phys.*, 2006, **78**, 159-178.
9. E. E. Meyer, K. J. Rosenberg and J. Israelachvili, *Proc. Natl. Acad. Sci. U. S. A.*, 2006, **103**, 15739-15746.
10. J. C. Rasaiah, S. Garde and G. Hummer, *Annu. Rev. Phys. Chem.*, 2008, **59**, 713-740.
11. B. J. Berne, J. D. Weeks and R. Zhou, *Annu. Rev. Phys. Chem.*, 2009, **60**, 85-103.
12. S. V. Buldyrev, P. Kumar, P. G. Debenedetti, P. J. Rossky and H. E. Stanley, *Proc. Natl. Acad. Sci. U. S. A.*, 2007, **104**, 20177-20182.
13. H.-J. Wang, X.-K. Xi, A. Kleinhammes and Y. Wu, *Science*, 2008, **322**, 80-83.
14. M. Ishizaki, H. Tanaka and K. Koga, *Phys. Chem. Chem. Phys.*, 2011, **13**, 2328-2334.
15. R. M. Lynden-Bell, N. Giovambattista, P. G. Debenedetti, T. Head-Gordon and P. J. Rossky, *Phys. Chem. Chem. Phys.*, 2011, **13**, 2748-2757.
16. A. Godec and F. Merzel, *J. Am. Chem. Soc.*, 2012, **134**, 17574-17581.
17. F. H. Stillinger, *Science*, 1980, **209**, 451-457.
18. S. Garde and A. J. Patel, *Proc. Natl. Acad. Sci. U. S. A.*, 2011, **108**, 16491-16492.
19. K. Lum, D. Chandler and J. D. Weeks, *J. Phys. Chem. B*, 1999, **103**, 4570-4577.
20. D. Chandler, *Nature*, 2005, **437**, 640-647.
21. S. Rajamani, T. M. Truskett and S. Garde, *Proc. Natl. Acad. Sci. U. S. A.*, 2005, **102**, 9475-9480.
22. J. Mittal and G. Hummer, *Proc. Natl. Acad. Sci. U. S. A.*, 2008, **105**, 20130-20135.
23. S. Suzuki, P. G. Green, R. E. Bumgarner, S. Dasgupta, W. A. Goddard and G. A. Blake, *Science*, 1992, **257**, 942-945.
24. R. N. Pribble and T. S. Zwier, *Science*, 1994, **265**, 75-79.
25. C. J. Gruenloh, J. R. Carney, C. A. Arrington, T. S. Zwier, S. Y. Fredericks and K. D. Jordan, *Science*, 1997, **276**, 1678-1681.
26. A. Laaksonen, P. Stilbs and R. E. Wasylishen, *J. Chem. Phys.*, 1998, **108**, 455-468.
27. Y. Ibrahim, E. Alsharaeh, K. Dias, M. Meot-Ner and M. S. El-Shall, *J. Am. Chem. Soc.*, 2004, **126**, 12766-12767.
28. C. Nieto-Draghi, J. Bonet Àvalos, O. Contreras, P. Ungerer and J. Ridard, *J. Chem. Phys.*, 2004, **121**, 10566-10576.
29. T. M. Raschke and M. Levitt, *J. Phys. Chem. B*, 2004, **108**, 13492-13500.
30. T. M. Raschke and M. Levitt, *Proc. Natl. Acad. Sci. U. S. A.*, 2005, **102**, 6777-6782.
31. M. Allesch, E. Schwegler and G. Galli, *J. Phys. Chem. B*, 2007, **111**, 1081-1089.
32. M. Allesch, F. C. Lightstone, E. Schwegler and G. Galli, *J. Chem. Phys.*, 2008, **128**, 014501.
33. P. N. Perera, K. R. Fega, C. Lawrence, E. J. Sundstrom, J. Tomlinson-Phillips and D. Ben-Amotz, *Proc. Natl. Acad. Sci. U. S. A.*, 2009, **106**, 12230-12234.
34. M. Kunieda, K. Nakaoka, Y. Liang, C. R. Miranda, A. Ueda, S. Takahashi, H. Okabe and T. Matsuoka, *J. Am. Chem. Soc.*, 2010, **132**, 18281-18286.
35. K. M. Lange, K. F. Hodeck, U. Schade and E. F. Aziz, *J. Phys. Chem. B*, 2010, **114**, 16997-17001.
36. T. C. Cheng, B. Bandyopadhyay, J. D. Mosley and M. A. Duncan, *J. Am. Chem. Soc.*, 2012, **134**,

13046-13055.
37. M. P. S. Mateus, N. Galamba and B. J. C. Cabral, *J. Chem. Phys.*, 2012, **136**, 014507.
38. P. Schravendijk and N. F. A. van der Vegt, *J. Chem. Theory Comput.*, 2005, **1**, 643-652.
39. K. P. Gierszal, J. G. Davis, M. D. Hands, D. S. Wilcox, L. V. Slipchenko and D. Ben-Amotz, *J. Phys. Chem. Lett.*, 2011, **2**, 2930-2933.
40. S. Furutaka and S.-i. Ikawa, *J. Chem. Phys.*, 1998, **108**, 1347-1351.
41. S. Furutaka and S.-i. Ikawa, *J. Chem. Phys.*, 1998, **108**, 5159-5160.
42. M. Besnard, Y. Danten and T. Tassaing, *J. Chem. Phys.*, 2000, **113**, 3741-3748.
43. Y. Jin and S.-i. Ikawa, *J. Chem. Phys.*, 2005, **122**, 024509.
44. A. Villa, C. Peter and N. F. A. van der Vegt, *J. Chem. Theory Comput.*, 2010, **6**, 2434-2444.
45. W. L. Jorgensen, J. Chandrasekhar, J. D. Madura, R. W. Impey and M. L. Klein, *J. Chem. Phys.*, 1983, **79**, 926-935.
46. W. L. Jorgensen and D. L. Severance, *J. Am. Chem. Soc.*, 1990, **112**, 4768-4774.
47. L. F. Molnar, X. He, B. Wang and K. M. Merz, *J. Chem. Phys.*, 2009, **131**, 065102.
48. C. D. Sherrill, T. Takatani and E. G. Hohenstein, *J. Phys. Chem. A*, 2009, **113**, 10146-10159.
49. C.-F. Fu and S. X. Tian, *J. Chem. Theory Comput.*, 2011, **7**, 2240-2252.
50. S. Nosé, *Mol. Phys.*, 1984, **52**, 255-268.
51. W. G. Hoover, *Phys. Rev. A*, 1985, **31**, 1695-1697.
52. M. Parrinello and A. Rahman, *J. Appl. Phys.*, 1981, **52**, 7182-7190.
53. S. Nosé and M. L. Klein, *Mol. Phys.*, 1983, **50**, 1055-1076.
54. U. Essmann, L. Perera, M. L. Berkowitz, T. Darden, H. Lee and L. G. Pedersen, *J. Chem. Phys.*, 1995, **103**, 8577-8593.
55. B. Hess, H. Bekker, H. J. C. Berendsen and J. G. E. M. Fraaije, *J. Comput. Chem.*, 1997, **18**, 1463-1472.
56. B. Hess, *J. Chem. Theory Comput.*, 2008, **4**, 116-122.
57. B. Hess, C. Kutzner, D. van der Spoel and E. Lindahl, *J. Chem. Theory Comput.*, 2008, **4**, 435-447.
58. A. Ben-Naim, *Molecular Theory of Solutions*, OUP Oxford, 2006.
59. P. Krüger, S. K. Schnell, D. Bedeaux, S. Kjelstrup, T. J. H. Vlugt and J.-M. Simon, *J. Phys. Chem. Lett.*, 2013, **4**, 235-238.
60. P. Ganguly and N. F. A. van der Vegt, *J. Chem. Theory Comput.*, 2013, **9**, 1347-1355.
61. R. Walser, A. E. Mark, W. F. van Gunsteren, M. Lauterbach and G. Wipff, *J. Chem. Phys.*, 2000, **112**, 10450-10459.
62. A. Baranyai and D. J. Evans, *Phys. Rev. A*, 1989, **40**, 3817-3822.
63. B. B. Mandelbrot, *Fractals: Form, Chance, and Dimension*, W. H. Freeman, 1977.
64. M. Y. Lin, H. M. Lindsay, D. A. Weitz, R. C. Ball, R. Klein and P. Meakin, *Nature*, 1989, **339**, 360-362.

Table 1. Force field parameters used in the molecular dynamics simulations.

molecule	atom	ε (kJ/mol)	σ (nm)	q (a.u.)
Water (TIP4P)	O	0.64852	0.315365	0.00
	H	0.00000	0.000000	0.52
	M[a]	0.00000	0.000000	−1.04
Benzene	C	0.29288	0.355	−0.115
(OPLS-AA)	H	0.12552	0.242	0.115

[a] M represents for the dummy atom in the TIP4P model.

Table 2. Summary of the systems simulated: the mole fraction for benzene (x_B), the number of benzene (N_B) and water (N_W) contained, and the side length of box (L_{eq}) for the equilibrated systems.

x_B	N_B	N_W	L_{eq} (nm)
0.0024	50	20724	8.5884
0.0036	75	20567	8.5832
0.0049	100	20388	8.5749
0.0050	103	20326	8.5708
0.0052	107	20351	8.5771
0.0054	110	20338	8.5769
0.0061	125	20253	8.5759
0.0074	150	20101	8.5722
0.0087	175	19945	8.5680
0.0100	200	19817	8.5673
0.0127	150	19483	8.5559
0.0154	300	19197	8.5508
0.0182	350	18843	8.5362
0.9706	4950	150	9.0645
0.9754	4960	125	9.0676
0.9803	4970	100	9.0698
0.9852	4980	75	9.0721
0.9901	5000	50	9.0814
0.9931	5000	35	9.1012
0.9950	5000	25	9.0789
0.9970	6600	20	9.9798

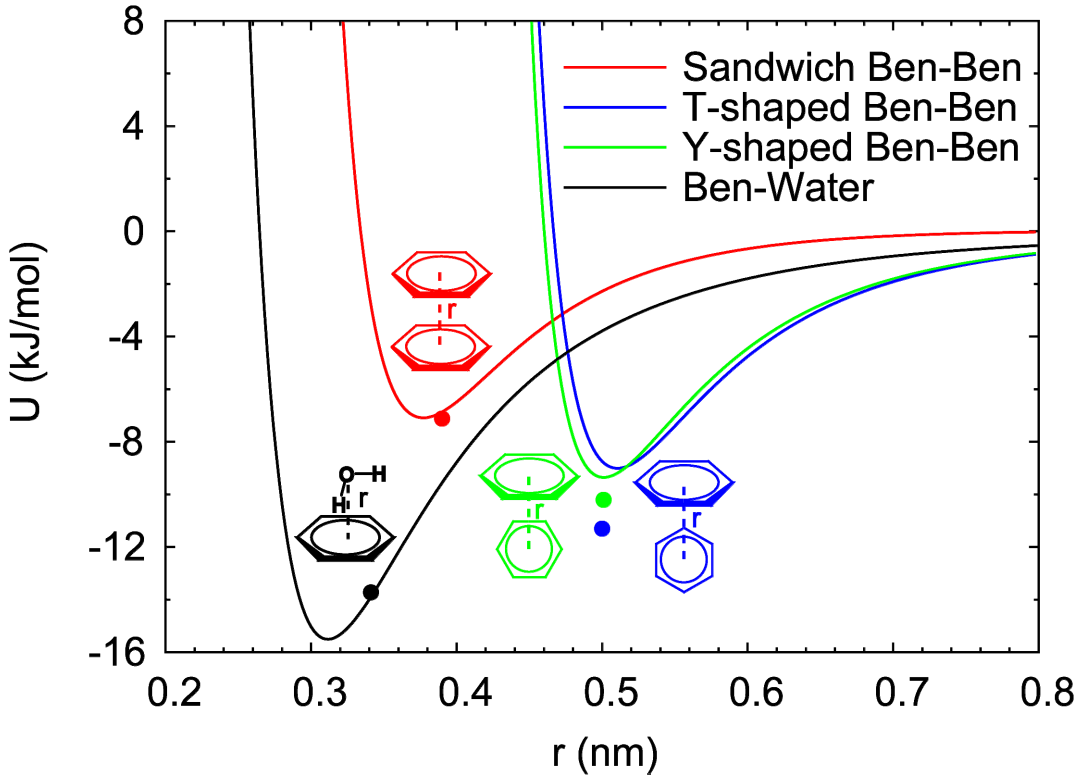

Figure 1. The potential energy curves of the dimers of benzene-benzene and benzene-water. The solid lines represent the intermolecular interactions predicted with the force fields; and the points are the results of the high-level quantum chemistry calculations (cited from refs. 47 and 48).

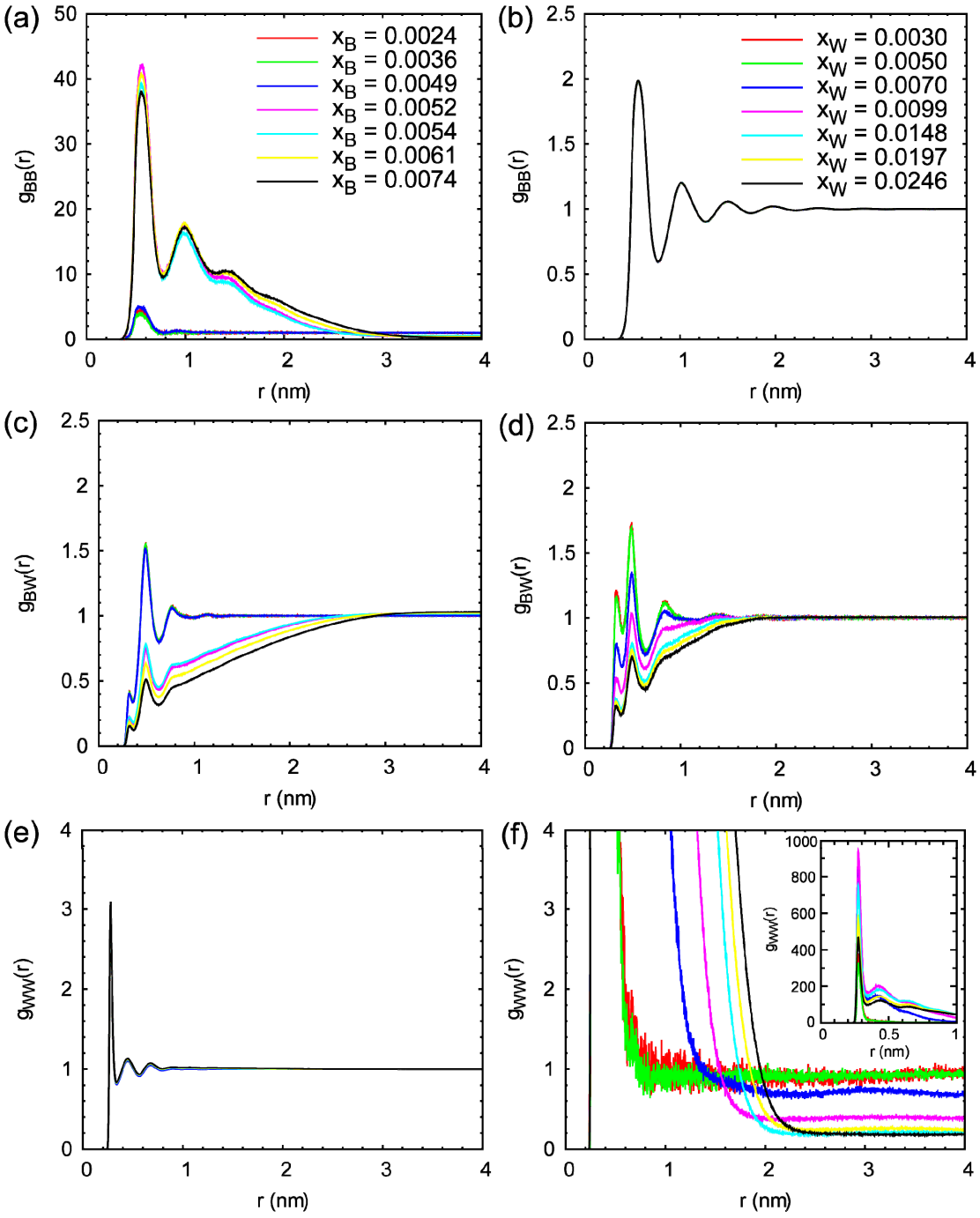

Figure 2. Radial distribution function [g_{ij}, i, j = B (benzene), W (water)] as a function of the distance between the centers of molecular mass: in the left column, for the water-rich mixtures with the legend shown in (a); in the right column, for the benzene-rich mixtures with the legend shown in (b).

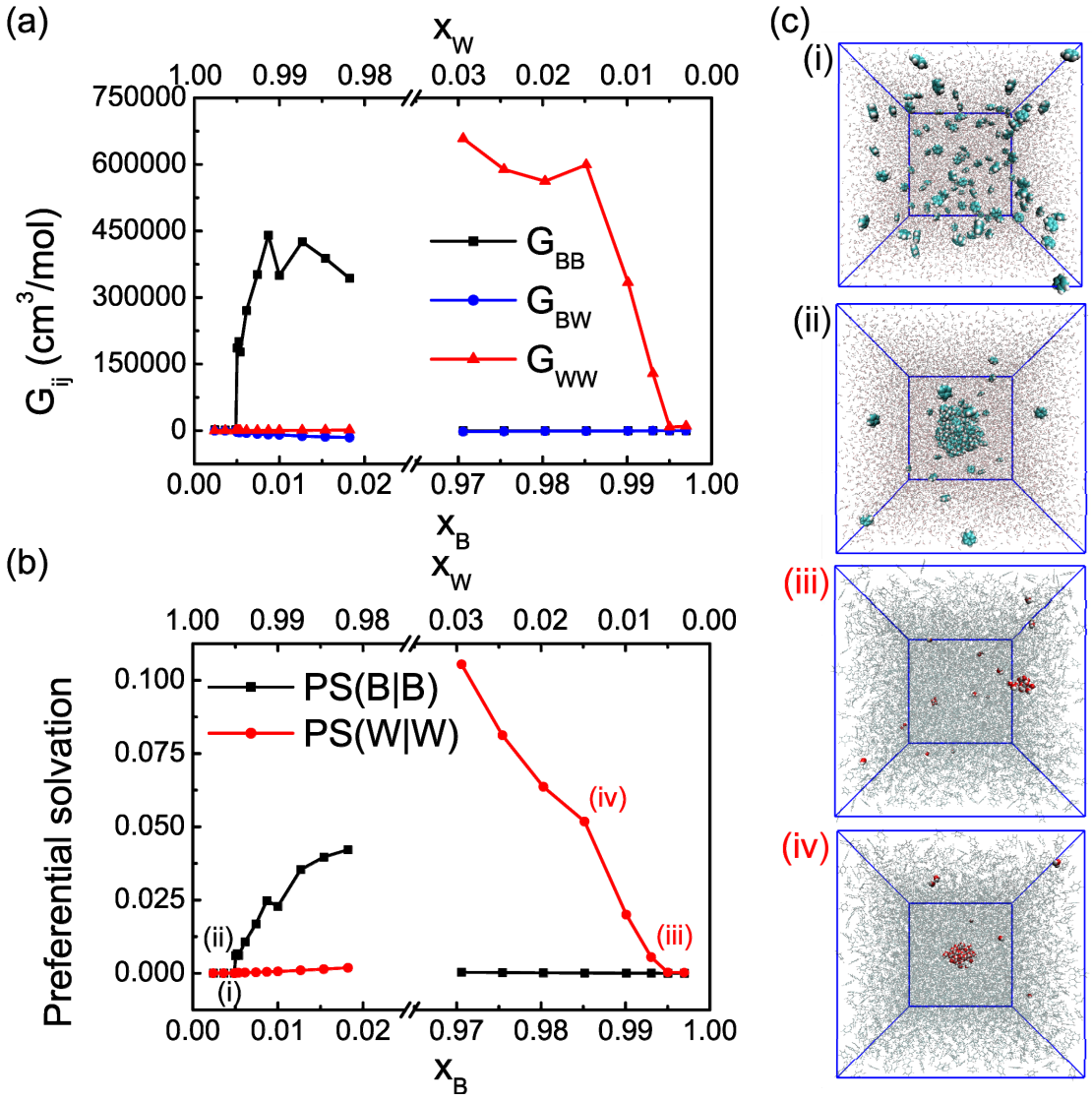

Figure 3. Kirkwood-Buff integral (a) and preferential solvation (b) in terms of the mole fraction of benzene (x_B) or water (x_W). (c) Snapshots of the equilibrium benzene-water mixture with four different mole fractions (noted in b): i, x_B = 0.0049; ii, x_B = 0.0052; iii, x_B = 0.9930; and iv, x_B = 0.9852.

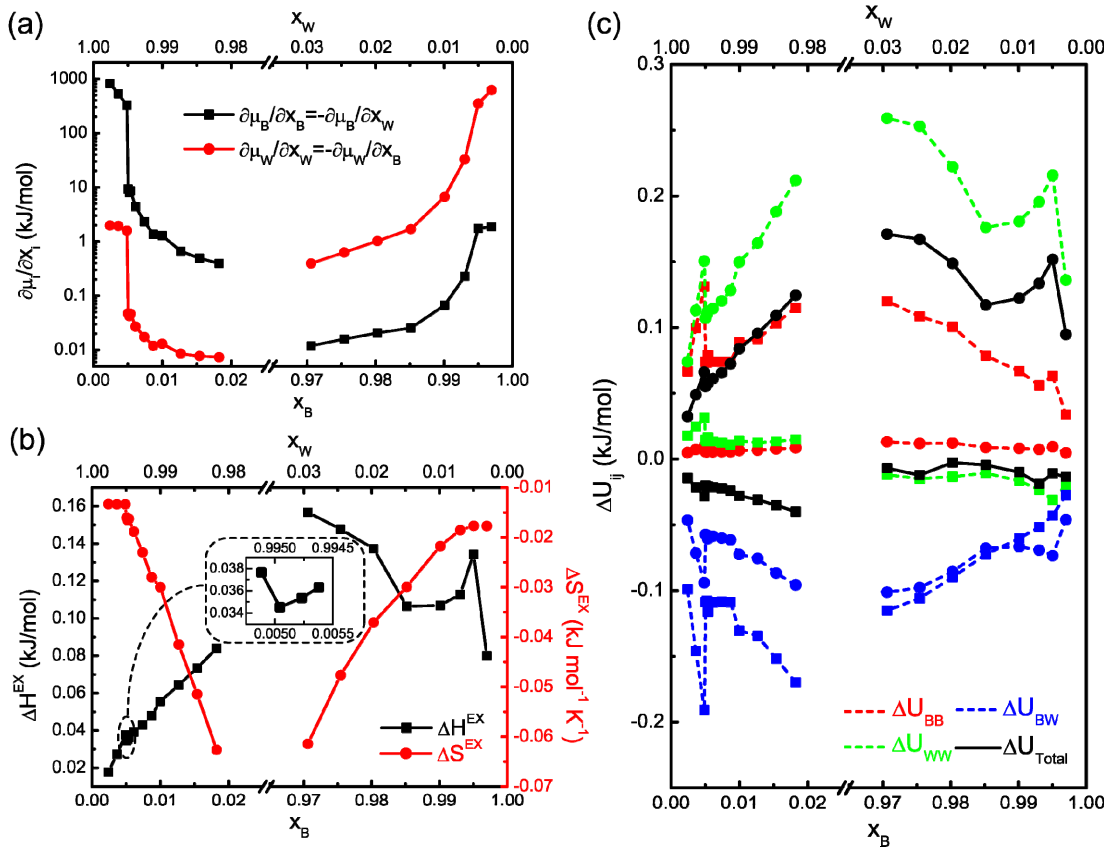

Figure 4. (a) Derivatives of the chemical potential (μ) with respect to the mole fraction. (b) The excess enthalpy (ΔH^{EX}) and excess entropy (ΔS^{EX}) of mixing as functions of the mole fraction. (c) Total intermolecular interaction energy (ΔU_{total}) and its different components as functions of the mole fraction of benzene or water; Square and circle labels represent the contributions of the Lennard-Jones and coulombic interactions, respectively.

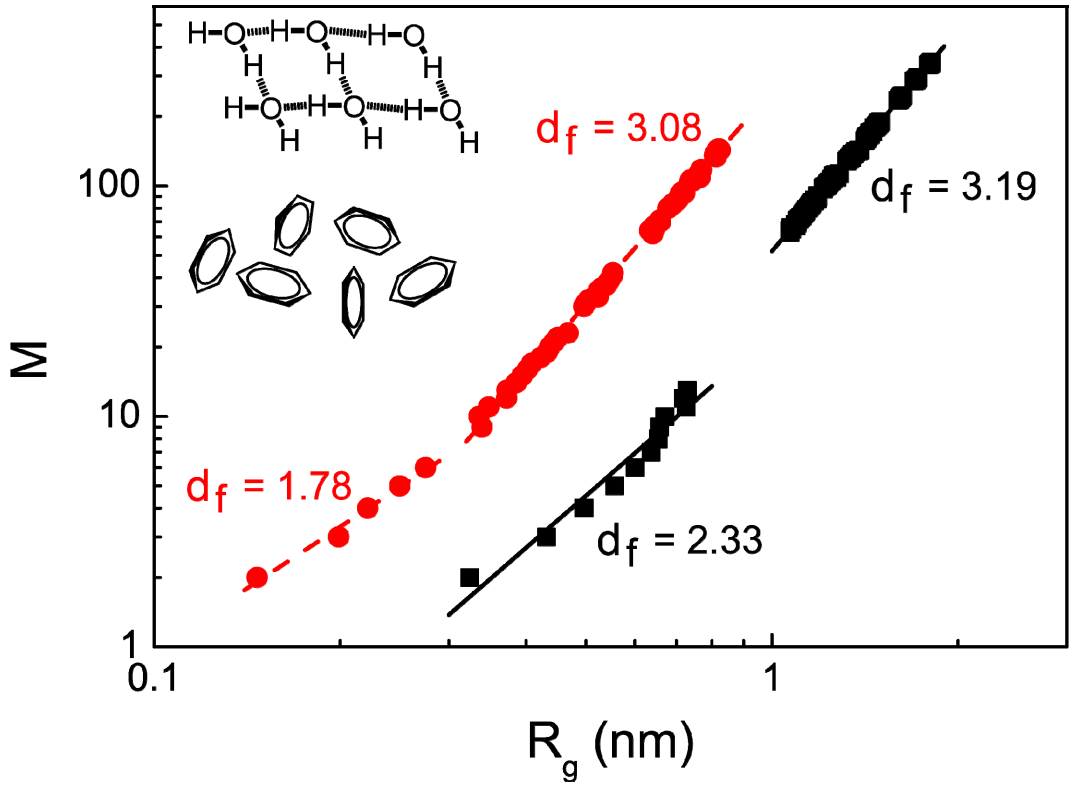

Figure 5. Cluster size M (the number of molecules contained in a cluster) as functions of the radius of gyration R_g. Black squares (■) and red circles (●) represent the results for benzene and water, respectively. The fitting lines (solid for benzene and dashed for water) are obtained with the relationship $M \propto R_g^{d_f}$. The inserted panels show the quasi planar aggregations of benzene and water molecules in the small clusters.

TOC